coatings

MDPI

Article

Tuning the electrical properties of tungsten oxide thin films deposited by reactive magnetron sputtering

Joël-Igor N'Djoré [1, 2], Moussa Grafouté[1], Younes Makoudi[2], Waël Hourani[2], Christophe Rousselot[2,*]

[1] Université Félix Houphouët Boigny, Laboratoire de Technologie, UFR SSMT 22, BP 258 Abidjan, Côte d'Ivoire ; joelndjore@outlook.fr (J.-I. N.) ; gramouss@hotmail.com (M.G.)
[2] Université de Franche Comté, Institut FEMTO-ST (CNRS/UFC/ENSMM/UTBM), Département MN2S, BP 71427, F-25211 Montbéliard cedex, France ; younes.makoudi@univ-fcomte.fr (Y.M.); wael.hourani@univ-fcomte.fr (W.H); christophe.rousselot@univ-fcomte.fr (C.R.)
* Correspondence: christophe.rousselot@univ-fcomte.fr; Tel . : (+33) 381 994 714)

Abstract: The tungsten oxide films have been deposited onto glass and silicon substrates using reactive magnetron sputtering. The correlation between the deposition process, chemical composition, optical and electrical properties was studied. The study of the system [W-Ar-O_2] hysteresis permitted us to gather the films into 4 zones which were delimited by different oxygen flow rate intervals. The identification of these zones was confirmed by the deposition rate, target voltage, chemical composition and electrical properties of the films. Electrical measurements were conducted by the 4 probes method and the mercury capacitance meter probe. A gradual evolution of capacitance-voltage curves of Metal-Oxide-Semiconductor structures with the WO_x thin film as the oxide layer was globally observed, with increasing oxygen flow rate. Ions density (N_{ss}) and flatband voltage (V_{fb}) evolved inversely according to oxygen flow rate. N_{ss} and V_{fb} evolution versus oxygen flow rate increase, reflects an improvement of oxygen stoichiometry in WO_x films. Also, WO_x/Si interface trap density distribution (D_{it}) was studied by Terman method. It was observed that films close to stoichiometry, i.e., WO_2 or WO_3, showed the lowest values of D_{it} and N_{ss}.

Keywords: reactive sputtering; tungsten oxide films; Metal-Oxide-Semiconductor structures; electrical properties; optical properties

Citation: Lastname, F.; Lastname, F.; Lastname, F. Title. *Coatings* **2022**, *12*, x. https://doi.org/10.3390/xxxxx

Academic Editor: Firstname Lastname

Received: date
Accepted: date
Published: date

Publisher's Note: MDPI stays neutral with regard to jurisdictional claims in published maps and institutional affiliations.

Copyright: © 2022 by the authors. Submitted for possible open access publication under the terms and conditions of the Creative Commons Attribution (CC BY) license (https://creativecommons.org/licenses/by/4.0/).

1. Introduction

As semiconductors technology advances, applications in the fields of microelectronics, optoelectronics, mechanics and decoration for instance, have been increased. In this respect, transition metal oxides represent an attracting class of material widely studied because of their wide range of physical and chemical properties. Among them, tungsten trioxide (WO_3) is one of the most attractive oxide for which it is well known that the oxygen to metal concentration ratio can be modified in order to obtain a conductive, semiconductor or insulating behavior, according to the oxygen quantity in the film [1]. WO_3 is easily reducible with several possible oxidation states for the tungsten atom and its sub-stoichiometry or over-stoichiometry modifies its chemical and physical properties. For this reason,WO_3 shows promising properties for applications in several important sustainable technologies, such as smart windows, anti-dazzle mirrors, gas sensors, information displays, humidity sensors, electrochromic devices, photocatalyst for air cleaning and water splitting [2–6]. Commonly used WO_3 thin film synthesis techniques are thermal evaporation [7], the sol-gel method [8], electrodeposition [9], DC (Direct Current) or RF (Radio Frequency) magnetron sputtering [10,11].

Studies of optical and electrical properties as a function of chemical composition reveal that WO_x thin films gradually evolve from reflective to transparent and from conductors to electrical insulators with the increasing of oxygen quantity in these films [10,12,13]

Generally, WO_x thin films electrical properties are studied with the Van Der Paw method also called 4-probes method. This method quickly reaches its limits when O-rich WO_x films become resistive [13]. Some authors use Hall effect measurements to establish electrical properties, such as mobility and charge carrier's concentration in tungsten oxide thin films [13,14]. Another alternative is to use the mercury probe for these types of samples. A MOS (Metal-Oxide-Semiconductor) structure is necessary in this case, and WO_x plays the role of the oxide. WO_x is a promising interfacial material for MOS-type devices because of its remarkable electrical, optical, thermal and chemical stability, compared to other oxide-type materials [15–17]. Recently, Baltakesmez et al. [18] showed the temperature influence on capacitance-voltage (C-V) curves characteristics, of $W/WO_3/Si$ structures for WO_3 different films. Also, Tutov [6] studied the C-V electrical characteristics of the $Al/WO_3/Si$ structure used as a humidity sensor.

However few works on the study of WO_3 electrical properties by measuring the MOS structure capacitance have been reported. The effect of oxygen content variation in WO_x thin films on electrical properties obtained by these capacitance measurements on a MOS structure has not been studied yet. Indeed, the characteristic curve C-V of MOS structures can give a diversity of information such as the density of ions in the oxide and at the oxide/semiconductor interface (N_{ss}), the flatband voltage (V_{fb}) and the interface trap density distribution (D_{it}).

In this work, WO_x thin films with different oxygen contents were synthesized by DC magnetron sputtering process. The main objective of this paper will be to establish the correlation between the evolution of WO_x films stoichiometry, and their electrical properties obtained from C-V characteristic curves of MOS ($Hg/WO_x/Si$) structures. Then, a more global correlation with the deposition process parameters and WO_x films physico-chemical properties will be proposed.

The paper is organized as follows. In section 2 we will describe the material and the experimental methods used. Section 3 will be devoted to the experimental results. We will start with the results of the deposits and the hysteresis, then the chemical composition followed by the optical properties, and finally the electrical properties. We will focus in particular on these electrical properties, because of the unusual method used and the important quantity of results to explain.

Finally, in section 4, the comparison of our results with those of the literature allows us to gather the synthesis of WO_x films in 4 zones, according to the oxygen flow rate used during the reactive sputtering process of a tungsten target. This delimitation of the different zones is discussed on the basis of the results of reactivity of O_2 with respect of tungsten target, the deposition rate, the target voltage, the chemical composition and the electrical properties of the films.

2. Materials and Methods

2.1. WO_x films synthesis conditions

WO_x-based films were deposited by DC (Direct Current) magnetron sputtering conventional process. Films deposition is achieved in an Alliance Concept AC 450 reactor with a vacuum chamber volume of 70 L. This chamber was evacuated with a turbomolecular pump backed by a mechanical pump leading to an ultimate pressure in the order of

$1x10^{-4}$ Pa. A W target (purity 99.9% and diameter 2′′) was fixed at 60 mm from the center of the substrate holder. The target was DC sputtered in Ar-O_2 atmosphere with a constant current of 100 mA. A pre-sputtering was applied during 15 min in order to remove the contamination on the target surface and to stabilize the reactive sputtering process before each deposition. A pumping speed of 10 L.s^{-1} was used in order to achieved a constant argon pressure of 0.41Pa. And then, different constant oxygen flow rates were used to deposit, at room temperature, amorphous WO_x films on standard microscope glass and silicon substrates. Before each deposition, these substrates were cleaned with ethanol and dried at room temperature. The n-type Si wafer (100) with resistivity of ~1-20 Ω.cm and a carrier concentration of ~ 10^{14}-10^{15} cm^{-3} was used for MOS studies.

2.2. Characterizations

Films chemical composition was determined by EDS (Energy Dispersive X-Ray Spectroscopy). EDS analysis were carried out with an OXFORD detector in the FEG JEOL 7610 F microscope, in order to determine the atomic concentrations of oxygen and tungsten in films. The EDS analysis carried out with an acceleration voltage of 5kV and a current of approximately 100 nA, allows the quantitative analysis from the signals of the Kα-line (0.525 eV) for the oxygen and of the Mα-line (1.775 eV) for the tungsten. For chemical analysis by EDS, all films were deposited on silicon substrates with thicknesses of approximately 500 nm (Table 1). WO_x film thicknesses were measured using a Dektak 3030 profilometer. Their deposition rate was determined from film thickness measurements and deposition time.

Q O_2 (sccm)	Total pressure (Pa)	Oxygen partial pressure (Pa)	Target voltage (V)	Film thickness (nm)
0.00	0.41	0.00	408	350
1.20	0.45	0.04	666	589
1.65	0.53	0.12	716	582
1.95	0.61	0.20	710	565
2.50	0.73	0.32	687	513
3.00	0.83	0.42	673	507
4.50	1.13	0.72	613	500
6.00	1.37	0.96	594	502
8.00	1.70	1.29	576	528
11.00	2.10	1.69	560	481

14.00	2.60	2.19	560	487

Table 1. Constant values of total and oxygen partial pressure and target voltage during the sputtering process for different oxygen flow rates. Experimental measurements of thickness achieved after WO_x deposition on glass substrates.

Optical properties study was carried out with a Perkin Elmer lambda 950 spectrophotometer and the evolution of optical transmittance is monitored in the wavelength range from 200 to 1,100 nm. Films were deposited onto glass substrates with a thickness of about 500 nm also (Table 1).

WO_x conductive films electrical resistivity was determined by the 4-probes method thanks to a JANDEL device at room temperature. Various electric currents I, between 1 µA and 9000 µA pass through the thin film, then the corresponding electrical voltage is recorded for each current value. The electrical resistivity is an average of resistivities calculated using the following equation:

$$\boldsymbol{\rho = 4.532 \times t \times \frac{U}{I}} \quad \text{(eq.1)}$$

with:

ϱ: resistivity (Ω.m), t: film thickness (m), U: electrical voltage (V) and I: electrical current (A).

WO_x thin films electrical properties were measured with a mercury probe capacitance meter, MDC (Materials Development Corporation). The capacitance meter is a device which enables MOS structures electrical characterizations by means of a capillary mercury (Hg) probe. The capillary mercury probe allows the deposition of a temporary grid in order to establish a metallic contact on the oxide surface. In this work framework, the MOS structures have the following configuration: Hg/WO_x/Si. The schematic diagram of the mercury probe capacitance meter is shown in the scheme I.

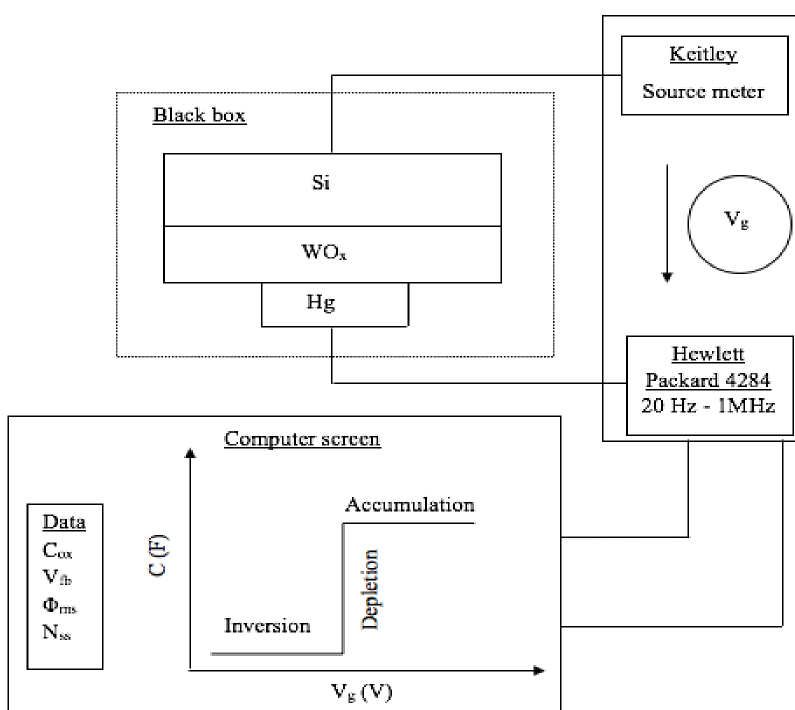

Scheme I. Schematic diagram of the experimental setup of the capacitance meter with a mercury probe. This device imposes a variable gate voltage on the MOS Hg / WO_x / Si structure, in order to measure the evolution of the capacitance of the MOS structure in the three regions of inversion, depletion and accumulation. The C-V curve is thus obtained with the parameters C_{ox}, V_{fb}, $\emptyset_{ms}$ and N_{ss} parameters. This curve shown in this diagram is considered theoretical or ideal due to the sudden change in capacitance in the depletion region.

The device is made of a black box or chamber, a Keithley generator coupled to a C-V data recorder Hewlett Packard 4284 A, a mercury probe controller model 802 to maintain Hg/WO_x contact and a computer. The MOS structure (Hg/WO_x/Si) is placed into the box which is kept close during the C-V measurements in order to avoid any influence of solar electromagnetic radiation. The Keithley generator varies the voltage across the MOS structure while the Hewlett Packard 4284 A measure the capacitance. This voltage, called the gate voltage, is the superposition of a high frequency alternative signal (AC) (1 MHz in our study) and a continuous signal (DC). The Keithley generator and the Packard 4284 A are connected to a computer fitted with a MDC Advanced Semiconductor Analysis Program to display measurement results and provide instructions to the device, respectively.

In practice, the first step of our measurement consists in determining the WO_x dielectric constant (k_{ox}) during the accumulation regime (Scheme I). To do so, we applied successively and in an increasing way, different gate voltages across the MOS structures (1 V, 2 V, 3 V, etc.). Then, we recorded the values taken by k_{ox} for each applied voltage. The k_{ox} of WO_x is determined when k_{ox} become constant vs gate voltage. We supply the k_{ox} value of the WO_x to the MDC Advanced Semiconductor Analysis Program and apply the gate voltage across the MOS structures in order to achieve the inversion, depletion and accumulation (Scheme I). The gate voltage interval in accumulation must correspond to the gate voltage interval for which k_{ox} is constant because a strong gate voltage in accumulation regime can destroy the oxide layer. We noticed that the applied gate voltage interval in accumulation depends strongly on the nature of the oxide, in particular on its stoichiometry. At the end of each C-V measurement, the values of the electrical parameters (C_{ox}, N_{ss}, V_{fb}, etc.) are displayed on the computer screen. Finally, once the C-V curve of the MOS structure is obtained, the D_{it} is systematically determined from C-V curves, using the "D_{it} by Terman" function contained in the MDC Advanced Semiconductor Analysis Program.

Electrical characteristics studied in this work from the C-V curves were V_{fb}, the D_{it} at WO_x/Si interface and N_{ss}. V_{fb} is the gate voltage (V_g) to be applied across the MOS structure so that the energy bands are flat. When energy bands are flat it means that there is no potential drop between the interface and the semiconductor volume. Thus, the surface potential is zero. D_{it} represents the number of electrically active traps per unit area and energy ($eV^{-1}cm^{-2}$), called interface states or interfaces traps, located at the WO_x/Si interface. In this work, D_{it} is determined by the Terman method [19,20]. This method is based on a high frequency measurement (100 KHz - 1 MHz) of C-V curves. As the gate voltage is a superposition of a high frequency AC signal and a DC signal [21], Terman assumes that the interface states cannot react to the AC signal, because of its high frequency. On the other hand, these interface states remain sensitive to the slow variation of the DC signal and are responsible for the "stretch - out" of the C-V curve measured, comparatively to the theoretical or ideal C-V curve. The interface states distribution is finally calculated by comparing the real and theoretical C-V curves through the following expression [22,23]

$$\mathbf{D_{it}} = \frac{\mathbf{C_{ox}}}{\mathbf{qA}} \frac{\mathbf{d(\Delta V_g)}}{\mathbf{d\Psi_s}} \quad \mathbf{(eq.\,2)}$$

Where:

$\Delta V_g = V_g$ (real) - V_g (theoretical) (V), D_{it}: the interface trap density distribution (states eV^{-1} cm^{-2}), q = 1.6 x 10^{-19} C: the elementary charge of the electron, A: the metal/oxide contact surface (m^2), C_{ox}: the capacitance of the oxide (F). and $\boldsymbol{\Psi_s}$: the surface potential of the semiconductor Si (V).

NB: The $\boldsymbol{\Psi_s}$ depend on the acceptor doping density of the substrate and the substrate intrinsic carrier density.

The N_{ss} represents total charges in the oxide and is determined by the following equations [21,22]:

$$\boldsymbol{N_{ss} = \frac{C_{ox}(\emptyset_{ms} - V_{fb})}{eA}} \quad (\mathbf{eq.3})$$

with

$$\boldsymbol{C_{ox} = \frac{k_{0x}\varepsilon_0 A}{t_{ox}}} \quad (\boldsymbol{eq.4}) \qquad \text{and} \qquad \boldsymbol{\emptyset_{ms} = \emptyset_m - \emptyset_s} \quad (\boldsymbol{eq.5})$$

where:

$\boldsymbol{C_{ox}}$: the measured accumulation capacitance (F), $\boldsymbol{\emptyset_{ms}}$: the metal-semiconductor work function (V), $\boldsymbol{\emptyset_m}$: the metal work function (V), $\boldsymbol{\emptyset_s}$: the semiconductor work function (V), $\boldsymbol{V_{fb}}$: the flatband voltage (V), $\mathbf{e}$: elementary charge (e $\approx$ 1.602 x 10^{-19} C), $\mathbf{A}$: the area of the MOS device (A = 4.89 x 10^{-7} m^2), $\boldsymbol{k_{0x}}$: the oxide dielectric constant, $\boldsymbol{\varepsilon_0}$: the permittivity of vacuum ($\boldsymbol{\varepsilon_0}$ $\approx$ 8.854 x 10^{-12} F m^{-1}) and $\boldsymbol{t_{ox}}$: the oxide thickness (m).

The $\boldsymbol{\emptyset_{ms}}$ depends not only on the semiconductor and the gate material, but also on the substrate doping type and density. Since the published literature shows variations of $\boldsymbol{\emptyset_{ms}}$ by as much as 0.5 V, it is obviously important to determine $\boldsymbol{\emptyset_{ms}}$ for a given process and not rely on published values [22]. In our study $\boldsymbol{\emptyset_{ms}}$ varied between 0.00132 V and 0.129 V.

As we can notice in equation 3, to calculate N_{ss} we need to know V_{fb}. However, V_{fb} cannot be directly obtained because it is necessary to calculate firstly the length of Debye (L_d) and then the flatband capacitance (C_{fb}) from the following expressions [21,22]:

$$\boldsymbol{L_d = \left(\frac{2k_s\varepsilon_0 KT}{e^2 N}\right)^{1/2}} \quad (\boldsymbol{eq.6}) \qquad \textbf{and} \qquad \boldsymbol{C_{fb} = \frac{k_{0x}\varepsilon_0 A}{t_{ox} + \left({k_{0x}}/{k_s}\right)L_d}} \quad \text{(eq.7)}$$

where:

$\boldsymbol{k_s}$: the Si dielectric constant, $\boldsymbol{k_{0x}}$: the oxide dielectric constant, $\boldsymbol{\varepsilon_0}$: the permittivity of vacuum ($\boldsymbol{\varepsilon_0}$ $\approx$ 8.854 x 10^{-12} F m^{-1}), $\boldsymbol{K}$: Boltzmann constant ($\boldsymbol{K}$ $\approx$1.38 x 10^{-23} J K^{-1}), $\boldsymbol{T}$: sample temperature (K), $\boldsymbol{N}$: the doping of Si ($\boldsymbol{N}$ $\approx$ 10^{14}-10^{15} cm^{-3}), $\boldsymbol{A}$: the area of the MOS device (A = 4.89 x 10^{-7} m^2), $\boldsymbol{t_{ox}}$: the oxide thickness (m).

V_{fb} is determined from C_{fb} and the C-V curve, by linear interpolation. All WO_x films deposited on Si for electrical properties study by MOS have a known thickness of about 200 nm. All the equations listed above were also found in our mercury probe capacitance meter device manual and are confirmed by references 21, 22 and 23.

3. Results and discussions

3.1. Reactivity of O_2 with respect of W target

221

Before the deposition of WO_x thin films, we studied firstly the reactivity of O_2 with W for a constant argon pressure of 0.41 Pa. Therefore, the O_2 injected into the deposition chamber reacted mainly with the W target, W sputtered atoms flux and all the metals inside the deposition chamber. To assess the reactivity of O_2 with respect of W target in the [W-Ar-O_2] system, the total pressure in the deposition chamber and the W target voltage were measured systematically for different O_2 flow rate introduced in the deposition chamber. To do that, O_2 flow rate was gradually injected from 0 to 15.2 sccm, and then reduced back to 0 sccm. For each O_2 flow rate introduced, the corresponding total pressure and target voltage are recorded as shown in Figure 1.

222–230

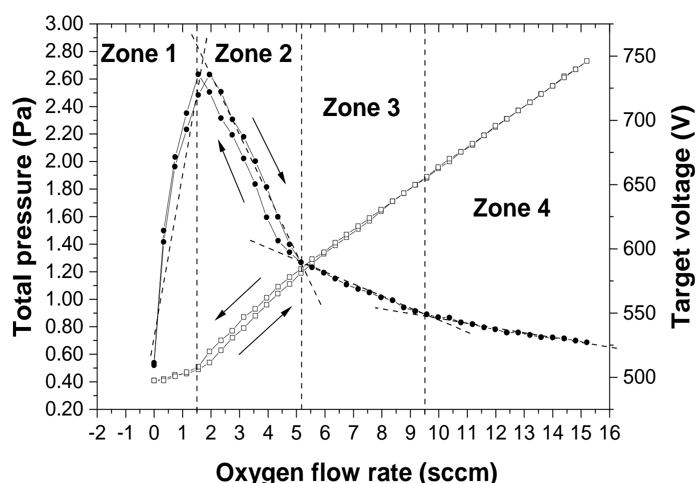

231

Figure 1. Hysteresis curves reflecting the total pressure (□) and target voltage (●) evolution as a function of O_2 flow rate when $Q(O_2)$ increases then decreases. The absolute errors on total pressure and target voltage are ± 0.01 Pa and ± 4 V, respectively.

232–234

According to the total pressure and the target voltage evolution as a function of O_2 flow rate introduced into the deposition reactor, 4 zones of O_2 reactivity with respect of W target are identified and presented in Figure 1. The limits between these different zones are indicative and more precisions about these zones will be given at the end of our study in section 4, considering the characterizations results for all WO_x films in this study.

235–239

- Zone 1 : $0\ sccm \leq Q(O_2) \leq 1.55\ sccm$

240

In zone 1, a small variation in the total pressure evolves from 0.41 Pa to 0.49 Pa for Q (O_2) = 0 sccm and Q (O_2) = 1.55 sccm, respectively. Contrary to the total pressure, the W target voltage increases abruptly from 509 V to about 720 V for Q (O_2) = 0 sccm and Q (O_2) = 1.55 sccm respectively. A low O_2 flow rate value is sufficient for the target voltage value to increase by almost 200 V between Q (O_2) = 0 sccm and Q (O_2) = 1.55 sccm. It should be noted that, like the total pressure, the changes in the target voltage values are almost identical when the oxygen flow rate in zone 1 increase and decrease and none hysteresis loop is observed.

241–248

- Zone 2 : $1.55\ sccm < Q(O_2) < 5.2\ sccm$

249

In this zone, the total pressure increases sharply from 0.49 Pa to 1.19 Pa, while the target voltage drops rapidly from about 720 V to 589 V as the oxygen flow rate increases from 1.55 sccm to 5.2 sccm, respectively. When the O_2 flow rate in zone 2 increases or

250–252

decreases, total pressure and target voltage values are respectively shifted, forming thus, a small hysteresis loop. This hysteresis loop could indicate an area of low instability in the system [W-Ar-O_2] [24,25].

- Zone 3: $5.2\ sccm < Q(O_2) < 9.5\ sccm$

In this oxygen flow rate interval, no hysteresis loop is observed on the target voltage when the oxygen flow rate increases and then decreases. The target voltage drops slowly and progressively from 589 V to 549 V when Q (O_2) increases. On the other hand, the total pressure increases systematically linearly from 1.19 to 1.9 when Q (O_2) increases, and presents a very slight shift during the decrease of Q (O_2), which seems to indicate incomplete oxidation of the target.

- Zone 4: Q (O_2) ≥ 9.5 sccm

When Q (O_2) ≥ 9.5 sccm, the total pressure and target voltage evolve linearly with the increase of Q (O_2). It shows that, no hysteresis loop is observed on the total pressure and the target voltage when the oxygen flow rate increases and then decreases, and allows us to suppose that the oxidation of the tungsten target is total, only in this zone 4.

The change in slope in the evolution of the W target voltage as a function of Q (O_2) between zone 3 and zone 4 reflects a change in the reactivity of O_2 with respect to tungsten target, while this change is not visible on the evolution of the pressure as a function of Q (O_2). These results allow us to separate zone 3 and zone 4, exhibiting O_2 reactivities with respect of the W target, which are close but nevertheless slightly different.

3.2. Synthesis of WO_x films

Several WO_x films were synthesized in the previous four zones for different oxygen flow rates. Oxygen flow rates, total and oxygen partial pressure, target voltage and film thickness values of synthesized WO_x films during this work are summarized in Table 1.

The WO_x deposition rate evolution as a function of O_2 flow rate ranging from 0 to 14 sccm, shown in Figure 2, is similar to the W target voltage evolution. An abrupt increase of the deposition rate from 14 nm min^{-1} to 48.5 nm min^{-1}, and of the target voltage from 408V to 716 V is observed for Q (O_2) included in zone 1. The sudden increase in W target voltage was also observed during the system hysteresis study (Figure 1). Indeed, when the target voltage increases, the Ar^+ ions in the plasma become more energetic and are more accelerated towards the tungsten target. Then, Ar^+ ions energies generate an increase in the W sputtering efficiency which is responsible for increase in the deposition rate. Also, these poorly oxygen enriched films are certainly less dense than tungsten films and therefore thicker for the same deposition time.

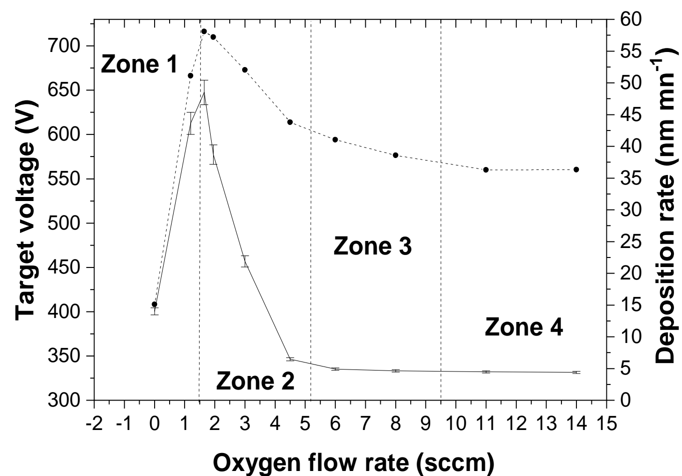

Figure 2. Evolution of W target voltage (dotted line) and deposition rate (line) during the synthesis of WO_x films at different oxygen flow rates from each of the 4 zones of $Q(O_2)$. The absolute errors on the target voltage is ± 4 V.

In zone 2, the W target voltage and the deposition rate drop significantly down to 610 V and 6.4 $nm.mn^{-1}$, respectively. In zones 3 and 4 the deposition rate and the W target voltage are very less influenced by the O_2 flow rate increase. In zone 3 the decreases of the deposition rate and the W target voltage are slow and effective while in zone 4 the W target voltage continues to slowly decrease due to the increase in total pressure while the deposition rate remains constant at 4.4 nm min^{-1}.

Decrease in deposition rate and W target voltage from zone 2 to zone 4 seems to be related to a progressive oxidation of the W target and with gradual change towards the compound sputtering mode. Indeed, the progressive oxidation of W target causes both a decrease in the sputtering efficiency of W-O compound formed on the target surface, compared to the W sputtering efficiency, and a decrease in the Ar^+ ions kinetic energy bombarding the target. The W oxide sputtering efficiency (Y_{Woxide}) can be estimated at around 0.15 for Ar^+ ions of 500 eV, from the equation $V_{dW}/V_{Woxide} = Y_W/Y_{Woxide}$ and knowing the deposition rates of W ($V_{d\,W} \approx 15$ nm min^{-1}), tungsten oxide ($V_{d\,Woxide} \approx 4.4$ nm min^{-1}), and tungsten sputtering efficiency ($Y_W \approx 0.5$ for Ar^+ ions of 500 eV). Several studies have shown that the ceramic target sputtering efficiency (oxidized target) is always lower compared to that of a metal target [26,27].

Also, the drop in the deposition rate can partially be explained by an important decrease in the mean free path of particles removed from the W target and transported under collisions to the substrate, when the oxygen flow and the total pressure increase in zone 2 and 3. Our results concerning the evolution of the deposition rate as a function of $Q(O_2)$ are comparable to those obtained by Yamamoto et al. [10] with a deposition rate which evolves from 10 to 35 nm min^{-1} for low $Q(O_2)$ then decreases as the oxygen flow rate increase to reach 2 nm min^{-1} when the W target is completely oxidized.

3.3. Chemical composition

The effect of the oxygen flow rate on the chemical composition of the WO_x thin films, has been investigated. WO_x films chemical composition shown in Figure 3 is consistent with results obtained during the hysteresis study (Figure 1), the deposition rate and target

voltage (Figure 2). The atomic ratio O/W evolution of WO_x films confirms the determination of 4 zones.

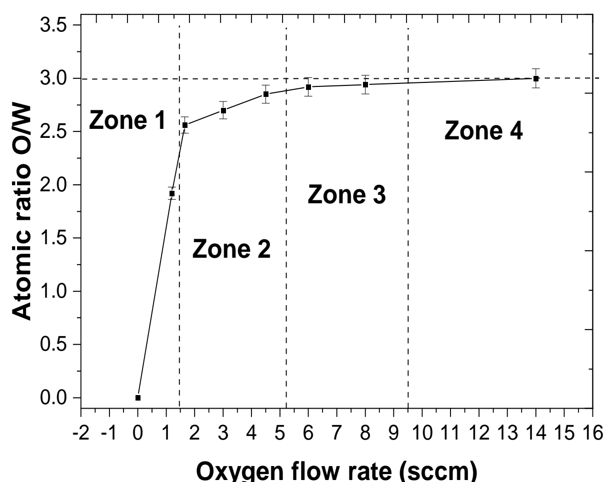

Figure 3. Evolution of the atomic ratio O/W as a function of O_2 flow rate.

In zone 1, a high reactivity of tungsten with oxygen is reflected by a rapid enrichment in oxygen for these films. It can be noted, in this zone 1, that the rapid linear increase in the O/W ratio reaches the value of 1.92 (close to stoichiometric compound WO_2 with an oxidation state of +4 for the tungsten atoms). In zones 2, 3 and 4, the atomic ratio O/W continues to increase more and more slowly to finally reach the value of 3 in zone 4, characteristic of the stochiometric formation of WO_3 with an oxidation state of +6 for the tungsten atoms. In zones 2 and 3, tungsten oxide Magnéli phases, which are generally sub-stoichiometric (WO_{3-y} with $y > 0$), could be formed. We could find in these zones, Magnéli phases such as $W_{26}O_{77}$ ($y = 0.04$), $W_{40}O_{116}$ ($y = 0.1$), $W_{20}O_{58}$ ($y = 0.1$), $W_{12}O_{34}$ ($y = 0.17$), $W_{18}O_{49}$ ($y = 0.28$), and other compounds with chemical formula W_mO_{3m-1} and W_mO_{3m-2} [28].

These results show that there is a close link between the parameters of the WO_x formation process, such as hysteresis curves, target voltage, deposition rate and the composition of deposited films. The oxygen flow rate choice allows the deposition of films with variable stoichiometry in oxygen and controllable by the total pressure or the target voltage. Films from zone 3 are highly oxidized but still sub-stoichiometric while those from zone 4 are totally oxidized and stoichiometric as predicted in Figure 2. WO_3 stoichiometric films are obtained only for oxygen flow rates from around 9.5 sccm and for target voltages close to 560V. This limit of $Q(O_2) \approx 9.5$ sccm, assumed at this stage of the study will be confirmed by the electrical characterizations and discussed in section 4.

Our results are comparable to those obtained by Parreira et al. [29] (target voltage and chemical composition). In particular, Parreira et al. obtained films with chemical composition $WO_{2.92}$, $WO_{2.86}$, $WO_{2.58}$ for target voltages of approximately 590 V, 620 V and 678 V, respectively.

3.4. Optical properties

3.4.1 Optical transmittance

Optical transmittance as a function of the wavelength of different WO_x thin films from zones 1 to 4 is shown in Figure 4 for various oxygen flow rates between 1.2 and 14

sccm. For comparison, glass optical transmittance is also measured (Figure 4.i). It is close to 92% in visible region and its absorption threshold is approximately 260 nm corresponding to a gap of about 4.8 eV.

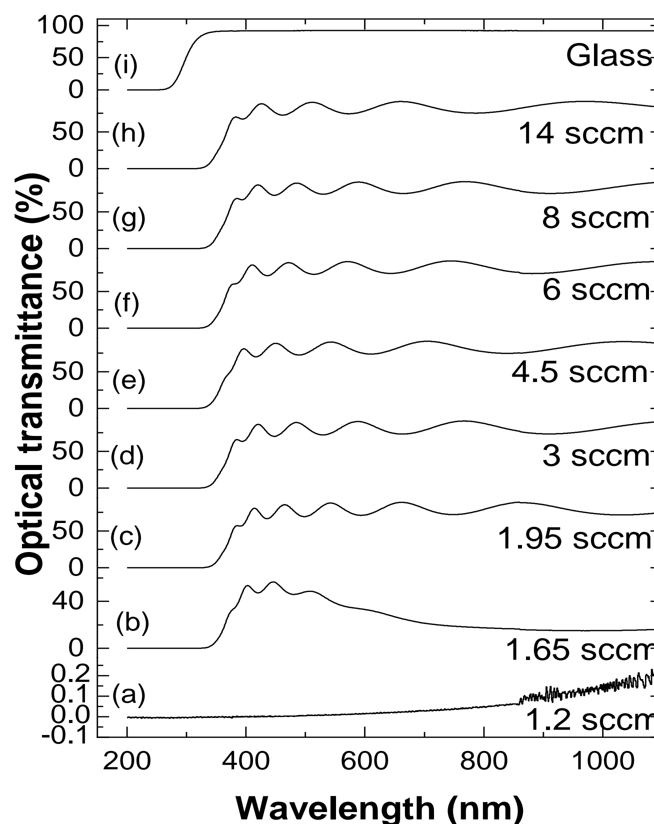

Figure 4. Effect of oxygen flow rate on optical transmittance spectra as a function of the wavelength of WO_x films deposited in zone 1 (a), zone 2 (b-e), zone 3 (f-g) and zone 4 (h). Glass optical transmittance as a function of the wavelength, is represented in Figure (i), as a reference transmittance spectrum. The absolute errors on optical transmittance is ± 0.05%.

The transmittance spectra of WO_x films deposited on glass for flow rates Q (O_2) ≥ 1.65 sccm are semi-transparent or transparent with interference fringes in the visible region and an absorption threshold beyond 310 nm (Figure 4 b-h). The absorption threshold for Q (O_2) = 1.65 sccm is approximately 325 nm and shifts to 315 nm with the increase in Q (O_2) up to 14 sccm. Strengthening of the W-O covalent bond as Q (O_2) increases disfavors inter-atomic electronic transfer and shifts the absorption threshold towards smaller UV wavelengths.

Figure 4 indicates various changes in optical transmittance of WO_x films from zone 1 to zone 4. The Film from zone 1 (Figure 4 a) exhibits the lowest optical transmittance in the wavelength range between 400 nm and 1,100 nm. In fact, the film deposited with Q (O_2) = 1.2 sccm, with chemical formula $WO_{1.92}$, is totally absorbent, very opaque with an average transmittance close to zero in visible region.

Films in zones 2 to 4 (Figure 4 b-h) evolves from semi-transparent to transparent. The film deposited with Q (O_2) = 1.65 sccm, with chemical formula $WO_{2.56}$, has an optical transmittance between 15% and 55% in the visible region with the appearance of a few interference fringes. This film presents a pronounced bluish appearance which is a characteristic of an under-stoichiometric tungsten oxide film, partially transparent, and having numerous oxygen vacancies associated to W^{4+} and W^{5+}, as already observed by Deb et al. [30]. This oxygen sub-stoichiometry favors the absorption of the photon and the electronic transfer between the oxygen valence band and the tungsten conduction band, at the origin of the bluing. But the electronic inter-valence transition between W^{4+} and W^{5+} can also give rise to this bluing. The others films have an optical transmittance between 60 % and 88 % for the film deposited with Q (O_2) = 1.95 sccm and between 65 % and 91 % for films deposited with Q (O_2) = 3 sccm to Q (O_2) = 14 sccm in the wavelength range between 400 nm and 1,100nm. Starting from this flow rate of Q (O_2) = 1.95 sccm the films of WO_x are totally transparent under our deposition conditions. The increase in Q (O_2) beyond 1.95 sccm accentuates the covalent character of the W-O bonds and therefore disadvantages not only the inter-atomic electronic transfer between O valence band and W conduction band but also the electronic inter-valence transition between the less present W^{4+} and W^{5+} ions in these transparent films.

Finally, from Figure 4, we can say that the improvement in the optical transmission of films obtained in zones 1 to 4 is essentially due to their progressive enrichment in oxygen. All transparent films are found in zones of high oxygen flow rate, i.e., from Q (O_2) > 1.65 sccm.

3.4.2 Optical band gap

The optical bandgap of WO_x thin film is determined by extrapolation of the increasing and linear part of the curve obtained from the Tauc method [31] according to the following equation :

$$(\alpha h\vartheta)^{1/n} = f(h\vartheta) \quad (eq. 8)$$

where α is the absorption coefficient and n is a number characterizing the electronic transition process, which can take the values 1/2, 3/2, 2 or 3 depending on whether the transition is direct permitted, direct forbidden, indirect permitted or indirect forbidden, respectively [32]. Researches of Hjelm et al. [33] showed that the WO_3 compounds have indirect permitted transitions with n = 2. The value of the optical band gap is then obtained by plotting the curve $(\alpha h\nu)^{1/2}$ as a function of the energy hν. The optical band gap corresponds to the abscissa of the intersection point between the abscissa axis and the linear increasing part of the curve which correspond to the region of maximum absorption [34], as shown in Figure 5 (see inset, for Q (O_2) = 8 sccm). The optical bandgap evolution as a function of the oxygen flow rate deposited from Q (O_2) = 1.65 sccm to 14 sccm is shown in Figure 5.

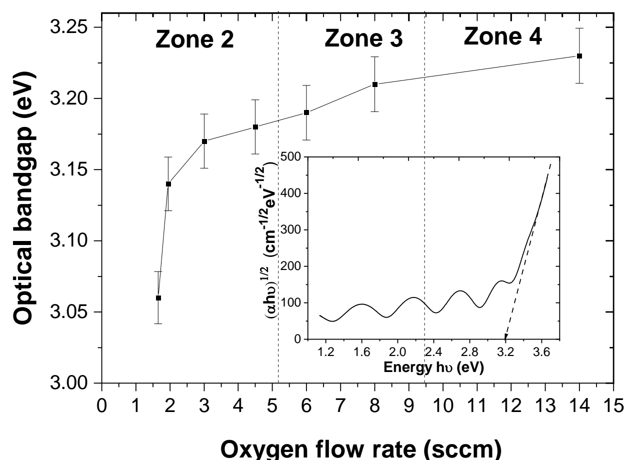

410

Figure 5. Evolution of the optical bandgap with respect to the oxygen flow rate of WO_x films deposited from Q (O_2) = 1.65 sccm to Q (O_2) = 14 sccm. Optical bandgap determination with Tauc method for Q (O_2) = 8 sccm is inserted. 411 412 413

414

According to Figure 5, optical bandgap increases from zone 2 to 4. In fact, the bandgap of WO_x films deposited between Q (O_2) = 1.65 sccm and Q (O_2) = 14 sccm evolves from 3.06 eV to 3.23 eV, respectively. We can assume that our deposited films are amorphous because these values are consistent with amorphous coatings structure [35,36]. In comparison, nanocrystallized WO_3 films optical bandgaps reported in literature are between 2.6 eV and 3 eV [30,37,38] generally. 415 416 417 418 419 420

The increase in the optical bandgap with Q (O_2) can be due to the enrichment in oxygen of WO_x films. For this reason, Migas et al. [39] showed by simulation that the increase of oxygen deficiency in WO_3 decreases the optical bandgap value. 421 422 423

As soon as, Q (O_2) increases, the transparent WO_x films contain reinforced W-O covalent bonds which will probably disadvantage the electronic transfers between the oxygen valence band and the tungsten conduction band and cause the increase of the optical band gap. On the other hand, for bluish films that are not completely transparent, the low optical band gap values certainly reflect an improvement in the inter-valence electronic transfer between the W^{4+} and W^{5+} cations, which are very present in these films which are poorer in oxygen. The evolution of Figure 5 is similar to that of Figure 3 and it confirms our proposed zone classification. 424 425 426 427 428 429 430 431

3.5. Electrical properties 432

3.5.1. Electrical resistivity 433

The electrical properties of the W-based conductive films deposited with Q (O_2) = 0 sccm, 1.2 sccm and 1.65 sccm were determined by conventional resistivity measurements according to the 4-probes method (see section 2.2). An increase in electrical resistivity with increasing oxygen flow rate was observed. The measured electrical resistivities are 5.30 x 10^{-5} Ω.cm, 1.45 x 10^{-2} Ω.cm and 25.4 Ω.cm for Q (O_2) = 0 sccm, 1.2 sccm and 1.65 sccm, respectively. The resistivity value of film deposited with Q (O_2) = 0 sccm close to 5 x 10^{-5} Ω.cm is consistent with the value in the literature. Indeed, during their study on electrical resistivity in W thin films sputter deposited by GLAD (Glancing Angle Deposition), 434 435 436 437 438 439 440 441

Beainoua et al. [40] calculated a resistivity at room temperature of W equal to 1.3 x 10^{-5} Ω.cm. We must precise that the electrical resistivity of tungsten bulk is 5.4 x 10^{-6} Ω.cm [41]. The calculated resistivity of W thin film is always higher than the one of W bulk. This is probably due to the porous columnar microstructure and the size of columns formed in the film which limit the diffusion of electrons.

In addition, the introduction of O_2 with a low flow rate immediately leads to a strong increase in the electrical resistivity which increases up to 2.54 x 10^{1} Ω.cm for Q (O_2) = 1.65 sccm. This strong increase in films electrical resistivity is caused by an oxygen enrichment. From Xu et al. and Goldfard et al. investigations [13,42], conductivity of tungsten oxide films are related to the O 2p-band relative intensity in the valence band spectral region. The O 2p-band grows with oxygen concentration, at the expense of the W d-band. As a result, the decrease of conductivity vs Q(O_2) is due to the reverse evolution of the O 2p and d-bands contribution to the intensity of the valence band region.

The electrical resistivity measurement-attribute a conductive behaviour to films deposited with Q (O_2) = 0 sccm and 1.2 sccm, and a semi-conductive behaviour to the one deposited with Q (O_2) = 1.65 sccm. These electrical properties are consistent with the literature and can be correlated to optical and chemical composition results. Indeed, according to the literature [43], it is observed that as deposited WO_{3-z} thin films exhibit different coloration aspects for different levels of oxygen deficiency : z > 0.5 films are metallic (absorbent) and conductive, z = 0.3-0.5 films are blue and conductive and z < 0.3 films are transparent and resistive, these findings being independent of the film preparation technique.

Above Q (O_2) = 1.65 sccm, films electrical properties are no more accessible with our 4-probe device and require the achievement of a MOS structure where the WO_x film constitutes the oxide material in the structure.

3.5.2. MOS structures

Figures 6 a-d shows the C-V characteristics curves at 1 MHz of Hg/WO_x/Si MOS structures. The C-V characteristic curve at 1 MHz of the Hg/SiO_2/Si reference MOS structure is inserted into the Figure 6 a. Figures 7 a and 7 b respectively represent the effect of oxygen flow rate on the D_{it} with respect to the energy variation in the silicon bandgap and the interface trap average density distribution ($D_{it-average}$) with respect to the oxygen flow rate, at the WO_x/Si interface. D_{it} is determined from the Terman method [19].

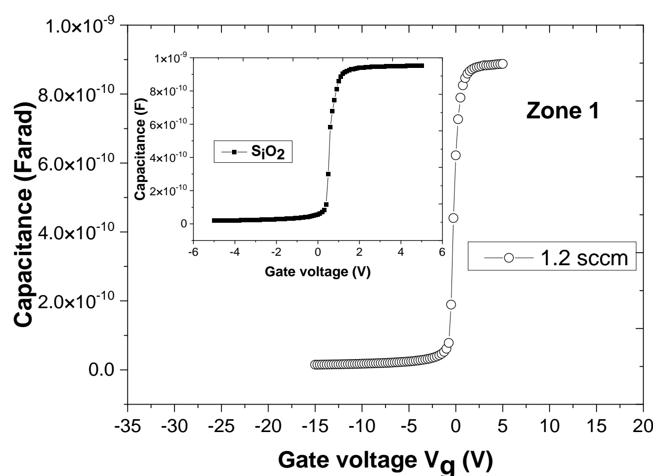

a 475

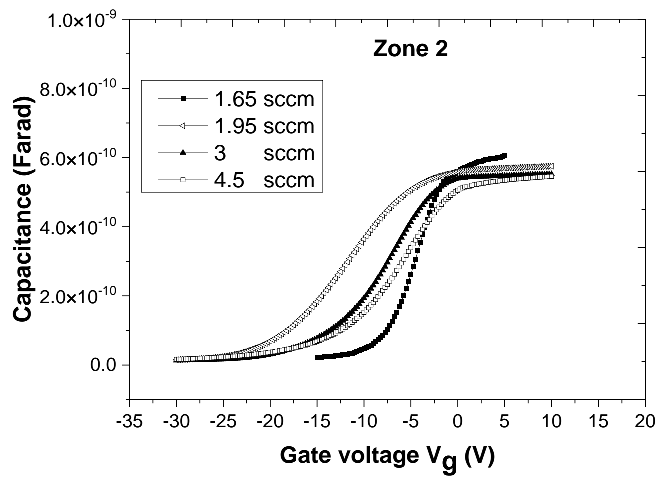

476

b 477

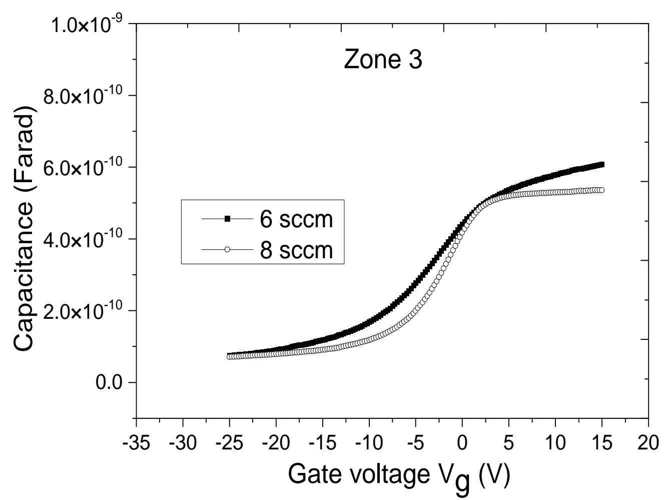

478

c 479

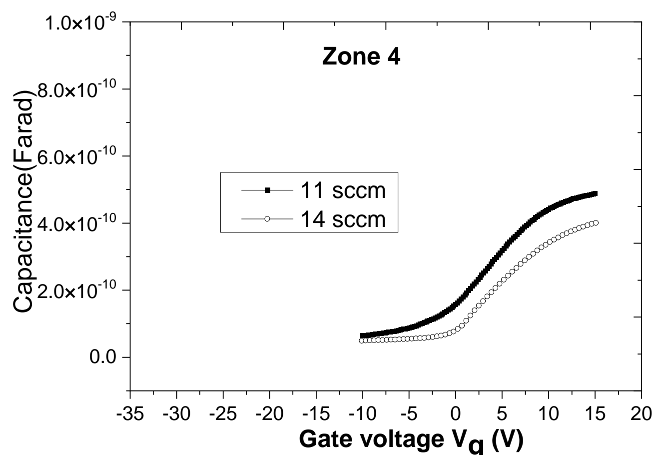

d

Figures 6 a-d. C-V characteristic curves at 1 MHz of Hg/WO_x/Si MOS structures obtained for WO_x films deposited with $0 < Q(O_2) \leq 14$ sccm included in zones 1 to 4. The C-V characteristic curve at 1 MHz of the Hg/SiO_2/Si reference MOS structure is presented in the insert. The absolute errors on capacitance measured is ± 0.005pF.

All C-V characteristic curves at 1 MHz of MOS capacitance (Figure 6 a-d) have three characteristic regions. From the left to the right, we can find regions of inversion, depletion and accumulation. As silicon is n-doped, the majority charge carriers are electrons. Indeed, in the region of accumulation, with $V_g > V_{fb}$, an accumulation of electrons occurs at the WO_x/Si interface by electrostatic influence. When the polarization of the MOS structure decreases, we access to the depletion region for which $V_t < V_g < V_{fb}$. V_t is called the threshold voltage and constitutes the limit between the region of inversion and the region of depletion. In the depletion region, electrons begin to leave the WO_x/Si interface in order to be repelled into the silicon volume. Finally, the inversion region is reached when $V_g < V_t$. In this region, all electrons are completely repelled from the WO_x/Si interface toward the silicon's volume by electrostatic influence in order to achieve an inversion layer which, normally contains only positive charges (holes).

The silica (SiO_2), is a native oxide layer, which is spontaneously formed on the Si surface. We did not perform any particular treatment other than cleaning the samples with alcohol, and our deposits were made on this interfacial SiO_2 native oxide layer, with a thickness of a few manometers (2-5 nm) [18]. This last is then negligible compared to the thickness of WO_x thin films (~200 nm). For this reason, and although there is a contribution of the SiO_2 native oxide layer, this contribution is the same for all samples and therefore we can assume that electrical properties results, are mostly dependent on WO_x thin films.

Figure 6 a (see inset) shows a sharp transition from the depletion regime (middle) to the accumulation regime (right) of the reference structure Hg/SiO_2/Si. This sudden variation reflects an excellent quality of the SiO_2/Si interface which contains less interface traps [44] . For this reason, Figure 7 a (n-Si Symbol: ◦) shows that the reference structure has the lowest interface trap density distribution. The measured interface trap average density distribution of the reference structure was estimated to be $4.08 \pm 0.32 \times 10^{11}$ states/cm^2/eV.

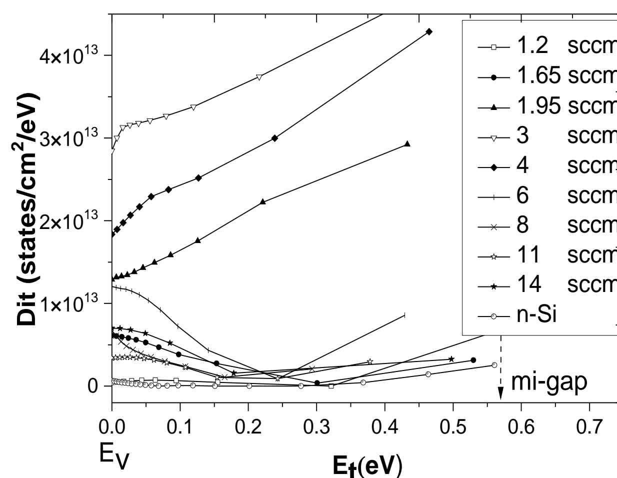

a

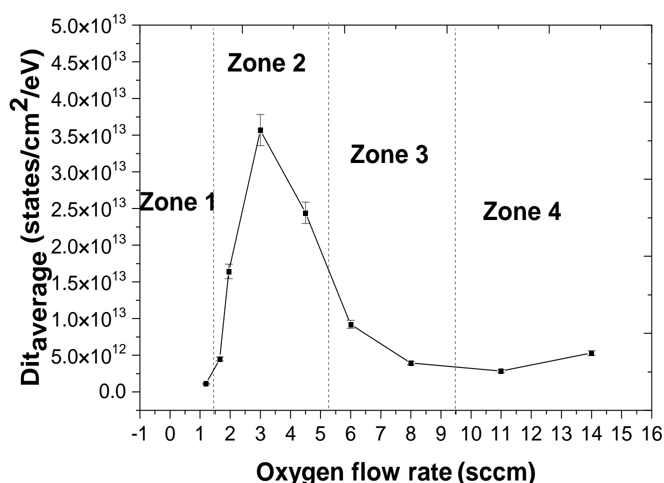

b

Figure 7 a-b. (a) Influence of oxygen flow rate on the D_{it} evolution, as a function of the energy variation in Si bandgap. The relative errors on D_{it} were evaluated ± 8%. (b) Evolution of the $D_{it\text{-}average}$, as a function of the oxygen flow rate.

A change in the shape of the C-V characteristics curves at 1 MHz of all Hg/WO_x/Si structures, compared to the reference structure, is globally observed in Figures 6 a-d. In zone 1 (Figure 6 a), the MOS structure obtained with Q(O_2) = 1.2 sccm with chemical formula $WO_{1.92}$, has a C-V characteristics curve which is similar to the one of the reference structure Hg/SiO_2/Si. Its transition from depletion to accumulation is abrupt. This MOS structure shows the lowest interface trap density distribution (Figure 7 a, 1.2 sccm Symbol: ▫) because it is close to stoichiometric WO_2. The interface trap average density of this structure (Q(O_2) = 1.2 sccm) is estimated to 1.13 ± 0.09 x 10^{12} states/cm²/eV (Figure 7 b).

In Zone 2 (Figure 6 b), the C-V characteristics curves of MOS structures obtained for films deposited with Q(O_2) = 1.65 sccm, 1.95 sccm, 3 sccm and 4.5 sccm tend to flatten in the depletion regime compared to the reference C-V curve. This phenomenon reflects effects occurring at the oxide/semiconductor interface and indicates a beginning of interface

quality degradation. Figure 7 a, shows that the interface trap density distribution at the WO_x/Si interface of MOS structures, for the WO_x films in zone 2 (1.55 sccm $< Q(O_2) <$ 5.2 sccm), increases significantly to reach a maximum D_{it} with $Q(O_2)$ = 3 sccm then decrease again for $Q(O_2)$ = 4.5 sccm. It presents a maximum for the MOS structure obtained with $Q(O_2)$ = 3 sccm with a chemical formula $WO_{2.70}$ and an interface trap average density of 3.57 ± 0.28 x 10^{13} states/cm^2/eV (Figure 7 b). The structural and/or lattice disagreement between these oxides and Si, or their non-stoichiometry which are the main causes of interface states, may be more important for these oxides films in this zone 2, for which atomic ratio O/W is far from 2 (WO_2) or 3 (WO_3) (Figure 3).

Zones 3 and 4 (Figure 6 c and d), for which Q (O_2) varies from 6 sccm to 14 sccm, do not show an abrupt transition from the depletion regime to the accumulation one neither. This also indicates a presence of traps at the WO_x/Si interface in these structures. Nevertheless, according to Figure 7 a, we can observe a fall of the interface trap density distribution in these zones. In zone 3, with $Q(O_2)$ = 6 sccm and 8 sccm, with chemical composition $WO_{2.92}$, $WO_{2.94}$, the interface trap average density decreases from 9.22 ± 0.74 x 10^{12} states/cm^2/eV to 3.95 ± 0.28 x 10^{12} states/cm^2/eV, respectively (Figure 7 b). Things occur as if, the interface traps decrease, when we tend towards the stoichiometry WO_3. In zone 4, the interface trap density becomes significantly lower for the MOS structure obtained for $Q(O_2)$ = 11 sccm with an interface trap average density equal to 2.86 ± 0.22.10^{12} states/cm^2/eV (Figure 7 b). The slight increase in the interface trap average density for the MOS structure obtained with $Q(O_2)$ = 14 sccm, equal to 5.31 ± 0.42 x 10^{12} states/cm^2/eV (Figure 7 b), may reflect the presence of oxygen atoms placed into interstitials site of this oxide. Finally, according to Figure 7 a, all interface trap density distributions are located in the lower part of the silicon bandgap. As a result, we can say that interface states are of donor-type [45].

A drop in the oxide capacitance (C_{ox}) is observed as we evolve from zone 1 (900 pF) to zone 4 (400 pF) (Figure 6 a-d). This could be related to the resistive nature of WO_x films deposited with higher oxygen flow rate [46] also linked to the covalent strengthening of W-O bonds when Q (O_2) increases. Also, in Figure 6 (a-d) it is important to note the different gate voltage ranges for the different zones. The choice of the gate voltage interval must be imperatively adapted to each oxide and beyond this interval WO_x films could be damaged

The effect of oxygen flow rate on the N_{ss} and the V_{fb} evolution is shown in Figure 8. This Figure shows the evolution of N_{ss} and V_{fb} as a function of oxygen flow rate. We can easily notice that these variations are opposite and different from one zone to another. The question that arises then, concerns the nature and the degree of oxidation of these ions. In fact, tungsten trioxide (WO_3) has a cubic perovskite-like structure based on corner-sharing WO_6 octahedra [28]. When deposited at room temperature, WO_3 is a monoclinic octahedron with W at the centre surrounded by six neighbouring oxygen, whereas the WO_2 can be considered as a quadrilateral with central W and four neighbouring oxygen [47]. Based on the literature [43,47], the most common valence states of W in as deposited WO_3 are W^{6+} and W^{4+} in strongly oxygen deficient material, but in less oxygen deficient material it may be formed both W^{4+}, W^{5+} and W^{6+}. Generally, W^{5+} is formed by electrochemical reduction of W^{6+} [28,48]. Therefore, the formation of W^{5+} valence state in as-deposited WO_3 films is unlikely but not impossible. The W^{5+} valence state can be viewed as the consequence of incomplete bonding between W and O in the octahedron [43,49].

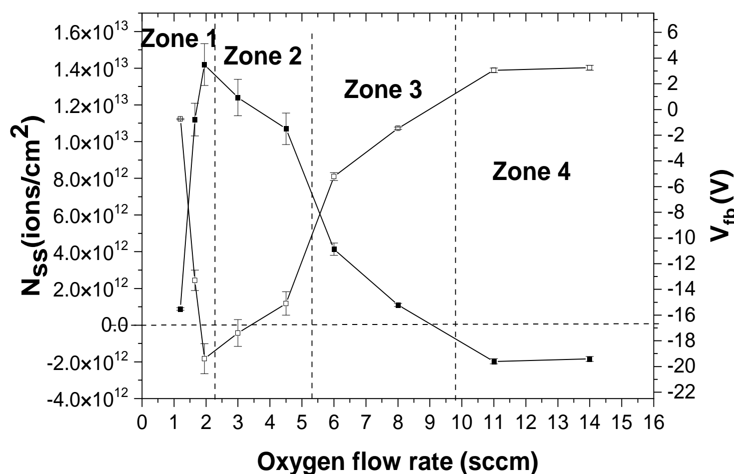

577

Figure 8. Influence of oxygen flow rate on the simultaneous evolution of N_{ss} (■) and V_{fb} (□) of Hg/WO_x/Si MOS structures for all WO_x films in zones 1 to 4. (La Zone 1 est mal délimitée car 1,65 sccm ne fait plus parti de cette zone) 578 579 580

In the other hand, and considering the oxygen vacancies in the films, the valence states of tungsten and oxygen, the N_{ss} showed in Figure 8 could reflect the evolution of charged species with general formula $(WO_{2-z})^{\varepsilon+}$ $0 \le z \le 2$ and $(WO_{3\pm z})^{\varepsilon\mp}$ $0 < z < 1$. The $(WO_{2-z})^{\varepsilon+}$are supposed to be positive species with regard to W^{4+} and O^{2-} valence states and dangling bond in the quadrilateral. In stoichiometric films, such as WO_2 and WO_3, we suppose $\varepsilon = 0$ because they are considered as neutral species. In sub-stoichiometric films, with general formula $(WO_{3-z})^{\varepsilon+}$ and $(WO_{2-z})^{\varepsilon+}$, ε may be positive (+) because of oxygen vacancies in the films, dangling bond and W^{4+}, W^{5+} and W^{6+} valence states. Finally, in over-stoichiometric films with general formula $(WO_{3+z})^{\varepsilon-}$, ε may be negative (-), because in these films there are no more oxygen vacancies and the excess of oxygen are placed into interstitial sites. 581–591

A close link between the evolution of N_{ss} and the evolution of C-V curves is observed. Indeed, according to Figure 6 a and b, in zones 1 and 2, when the oxygen flow rate increases from Q (O_2) = 1.2 sccm to Q(O_2) = 1.65 sccm, a shift of C-V curves and the flatband voltage towards negative gate voltage is observed. This shift towards negative gate voltages reflects a progressive increase of positive charges $(WO_{2-z})^{\varepsilon+}$ or $(WO_{3-z})^{\varepsilon+}$ present in the oxide [50], from Q(O_2) = 1.2 sccm to Q(O_2) = 1.65 sccm as shown in figure 8. In the film deposited with Q(O_2) = 1.2 sccm, with atomic ratio O/W of 1.92 ± 0.06, we could probably find a combination of WO_2 which are neutral species and a few amounts of $(WO_{2-z})^{\varepsilon+}$ which are positive species because of W^{4+} and O^{2-} valence states in the quadrilateral. N_{ss} is close to zero in the film deposited with Q(O_2) = 1.2 sccm perhaps because of an important neutral charge amount (WO_2) in this film. The film deposited with Q(O_2) = 1.65 sccm in zone 2, with atomic ratio O/W of 2.56 ± 0.08, is becoming a little bit transparent because of a possible combination of WO_2 and $(WO_{3-z})^{\varepsilon+}$. The $(WO_{3-z})^{\varepsilon+}$ positive charges may contain W^{6+} valence states which are responsible for transparent films. 592–605

In zone 2, the MOS structure obtained with Q(O_2) = 1.95 sccm, 3 sccm and 4.5 sccm (Figure 6 a), which shows the most shifted C-V curves toward negative gate voltages, presents the lowest flatband voltage (Figure 8). These films, with 2.60 ± 0.08 < atomic ratio O/W < 2.90 ± 0.09, may contain the maximum quantity of positive species $(WO_{3-z})^{\varepsilon+}$ and oxygen vacancies. We may find a combination of W^{4+} and W^{6+} valence states in these films. According to Figure 4 c-d-e, these films have an average optical transmission close to 80 606–611

% in the visible region reflecting that positive species $(WO_{3-z})^{\varepsilon+}$ with W^{6+} valence state, are predominant. From Q(O_2) = 6 sccm to Q(O_2) = 14 sccm, i.e., C-V curves and flatband voltage shift progressively from a negative gate voltage to a positive one (Figure 6 c-d). This C-V curves evolution reflects the decrease of positive species [50] $(WO_{3-z})^{\varepsilon+}$ amount in these oxides due to the fulfilment of oxygen vacancies when Q(O_2) increases from Q(O_2) = 1.95 sccm. Above Q(O_2) = 1.95 sccm, we may find combination of positive charges such as $(WO_{3-z})^{\varepsilon+}$ and neutral charges such as WO_3 and WO_2 with W^{6+}, W^{5+} and W^{4+} valence states. Since films in these regions present an average optical transmittance above 80 % in visible spectral region, we may assume that tungsten valence states W^{6+} are predominant compared to W^{4+} and W^{5+}.

Figure 8 shows negative values of N_{ss} and positive values of V_{fb} for both films deposited with Q(O_2) = 11 sccm and Q(O_2) = 14 sccm (zone 4). The values of N_{ss} and V_{fb}, which are almost constant, mean that negative charges are predominant in these films [50]. All the oxygen vacancies seem to be fulfilled by oxygen, so we can assume that we could no longer find positive charges $(WO_{3-z})^{\varepsilon+}$ in these films. Indeed, when all oxygen vacancies in WO_6 octahedra or WO_3 are fulfilled, the excess of oxygen flow rate, may generate O^{2-} ions which could be placed into interstitial sites between WO_6 octahedra in WO_3 films. In this situation, N_{ss} corresponds to negative species $(WO_{3+z})^{\varepsilon-}$ with W^{6+} valence states in the octahedra. In this zone 4, films are stoichiometric or over-stoichiometric according to results of the atomic ratio O/W (Figure 3).

According to Figure 8, V_{fb} and N_{ss} evolve inversely with respect to each other. Also, more the flatband voltage shifts towards positive gate voltages, the fewer positive charges are created in the oxide and the more negative charges created in the oxide are numerous. These observations can be correlated with the composition of the films (Figure 3). Indeed, for N_{ss} close to zero or negative, the films appear close to the stoichiometry or are stoichiometric or over stoichiometric.-For example, the film obtained with Q(O_2) = 1.2 sccm presents a N_{ss} close to zero with an atomic ratio O/W of 1.92 ± 0.06 close to WO_2. Otherwise, the film deposited with Q(O_2) = 14 sccm with atomic ratio O/W of 3 ± 0.09 close to WO_3, presents a negative value of N_{ss}. On the other hand, as soon as the N_{ss} increases, the atomic O/W ratio moves away from the stoichiometry either WO_2 or WO_3.

4. Description of the different WOx films zones formation

Based on the different trends observed on the W target voltage during the study of the system [W-Ar-O_2] hysteresis (Figure 1), chemical composition, optical and electrical properties, we classify the WO_x films formation process into 4 zones, contrarily to literature which propose 3 zones [10,12,13]. The system [W-Ar-O_2] hysteresis was not studied by these authors who suggested 3 zones of WO_x formation process. Otherwise, in agreement with these authors, we determined the same extreme zones, namely, zone 1 and zone 4 in our study. Also, the WO_x deposition rate evolution int this study is similar to Yamamoto et al. [10].

In the zone 1,$0\ sccm \leq Q(O_2) \leq 1.55\ sccm$, the W target is globally kept in the metallic state (metal target mode) despite the small amount of O_2 introduced into the deposit chamber. Indeed, the O_2 molecules injected into the deposit chamber are trapped by getter effect on the deposit chamber walls receiving tungsten, the polarized tungsten target and the sputtered tungsten atoms [10]. Because of this getter effect, a very weak variation of total pressure or O_2 partial pressure is observed during the increase and decrease of Q(O_2) in this region. This weak variation of oxygen pressure was also observed by Mohamed et al. [12]. In this metal target mode, the deposition rate and target voltage increase abruptly. This sudden increase in W target voltage for lower O_2 flow rate was also observed by Sadiki et al.[51]. For Yamamoto et al. [10], films formed in this region of metal target mode

are W, W_3O with appearance of WO_2 in films deposited at 500 °C. They are absorbent and electrically conductive. For Mohamed et al. [12], absorbent WO_x ($0 < x < 1.5$) films are formed but he did not synthesized films above $WO_{1.5}$ in this region. Regarding these results, we can say that our results are in accordance with these authors because we formed reflective or absorbent and conductive films W and $WO_{1.92}$ with $Q(O_2)$ = 0 and 1.2 sccm, respectively. For this WO_x film with $Q(O_2)$ =1.2 sccm and close to the stoichiometry of WO_2, the parameters V_{fb} and D_{it} are close to zero indicating respectively few charges created in the film and few defects at the WO_x/Si interface. However, due to the sub-stoichiometry of this $WO_{1.92}$ films, an excess of positives charges remains and the positive value of N_{ss} reflects this excess of positive charges in the volume.

The WO_x films sputtered deposited in the high O_2 flow rate zone 4 ($Q(O_2) \geq 9.5\ sccm$) presented the lowest and constant deposition rate (4.4 nm. min^{-1}) and W target voltage (560 V). This result reflects that the W target surface is totally coated with an oxide layer, i.e., totally polluted or oxidized. According to Yamamoto et al. [10], the W target is in an oxide target mode. For us, and according to our atomic ratio O/W and N_{ss} results, only stoichiometric WO_3 or over-stoichiometric WO_{3+z} ($z \geq 0$) are formed in this oxide target mode. All the WO_x films synthesized in this region are transparent and electrically resistive as we observed in our work. Electrical analysis of this oxide films indicated values $V_{fb} \geq 0$ and $N_{ss} \leq 0$ reflecting a saturation in O_2 in the films formed in this zone 4.

Between the metal target mode (zone 1) and the oxide target mode (zone 4), we find a transition zone (z_t). From this transition zone, the O_2 introduced in the deposition chamber exceeds the getter effect observed in zone 1. This transition zone is not clearly discussed in the literature. Indeed, Mohamed et al. [12] did not performed any sample in this region during their study contrary to Yamamoto et al. [10] and Xu et al. [13]. Also Mohamed et al. [12] performed their study with a constant total pressure of 1.2 Pa and Yamamoto et al. [10] with 5 mtorr (0.66 Pa). Xu et al. [13] synthesized WO_x films by periodically pulsing the O_2 flow rate in order to avalanche the reactive sputtering process between the metal target mode and the oxide target mode. As far as we are concerned, we synthesised WO_x films by varying the total pressure through the variation of the oxygen flow rate. Therefore, our total pressure varies from 0.4 to 1.8 Pa in this transition zone. For Yamamoto et al. [10], the W target is still kept in a metallic state (metal target mode) and WO_x ($2 \leq x < 3$) films are formed by the reaction of W and O atoms on the substrate surface, with the amount of O_2 molecules exceeding the getter effect. Their results are not supported by any chemical analysis measurement in this zone. Also, for Yamamoto et al. [10] et Xu et al [13], these WO_x ($2 \leq x < 3$) films are blue or semi-transparent. Films from this transition zone become resistive for Yamamoto et al. [10] or semi-conducting for Xu et al [13]. In our study, during the formation of WO_x ($2.56 \leq x \leq 2.94$) in the transition zone corresponding to $1.65 \leq Q(O_2) \leq 8$ sccm, we observed a decay of the deposition rate as observed by Yamamoto et al. [10] and a decay of the target voltage. This decay ~~reflecting~~ means that the W target is no more kept in its metallic state as supposed by Yamamoto et al. [10], but start oxidizing. In our opinion, the transition zone of WO_x ($2 \leq x < 3$) films, must end when the formation of stoichiometric WO_3 begins, i.e., from oxygen flow rate approximatively 9.5 sccm. Also, we remember that all transparent films are not necessarily stoichiometric WO_3 since some sub-stoichiometric films can be transparent as shown in our work in zones 2 to 4.

In the transition zone, we observed that films optical transmittance and electrical properties evolve from semi-transparent (%T < 50) and semi-conducting (for $WO_{2.56}$, $Q(O_2)$ = 1.65 sccm) to transparent (between 70 % to 90 % in visible region) and resistive for other films. By considering only these optical transmittance results as a function of the wavelength, we might think that this transition zone beyond 1.65 sccm, produces films with identical behaviour. However, several observations lead us to believe that these films are

not all identical. Indeed, films prepared for 1.65 sccm $<Q(O_2) \leq 4.5$ sccm have similar and different behaviours from films prepared with $6 \leq Q(O_2) \leq 8$ sccm. As an example, the deposition rate and target voltage drop very quickly from 1.65 sccm to 4.5 sccm then drops much slower to 8 sccm. There is a low hysteresis on total pressure and W target voltage between 1.55 sccm and 5.2 sccm and not visible beyond 5.2 sccm. The chemical composition increases quite strongly from 2.56 ± 0.08 to 2.85 ± 0.08 for $1.65 \leq Q(O_2) \leq 4.5$ sccm then more slowly from 2.85 ± 0.08 to 2.94 ± 0.09 for 4.5 $<Q(O_2) \leq 8$ sccm. The $N_{ss} > 0$ with high values for films with 1.65 sccm $\leq Q(O_2) \leq 4.5$ sccm reflecting an excess of positive charges for these films of greater sub-stoichiometry 2.56 ± 0.08 to 2.85 ± 0.08. But the lower values of N_{ss} determined for films with 4.5 sccm $<Q(O_2) \leq 8$ sccm reflect a small amount of positive charge associated with a very slight sub-stoichiometry 2.85 ± 0.08 to 2.94 ± 0.09. Based on these results, we propose to subdivide this transition zone WO_x ($2 \leq x < 3$) into 2 distinct zones, i.e., Zone 2 for 1.55 sccm $< Q(O_2) <$5.2 sccm and Zone 3 for 5.2 sccm $<Q(O_2) <$9.5 sccm. The zone 3 constitutes the end of the transition zone. That justifies the small variation observed in the data and in the trends proposed, in particular on the chemical composition, the deposition rate, the target voltage, etc. for films in these zones 3 and 4.

5. Conclusions

In this work, WO_x thin films were synthesized by the DC reactive magnetron sputtering method. Based on links observed between the system [W-Ar-O_2] hysteresis, the deposition rate, the target voltage, chemical composition and electrical properties, we proposed 4 zones of WO_x films formation, with different stoichiometries. Each zone is delimited by different oxygen flow rates.

In zone 1, delimited by $Q(O_2) \leq 1.55$ sccm, the deposition rate and the target voltage increase rapidly when oxygen flow rate increases. In this zone 1, films are progressively opaque and bluish with the increase of $Q(O_2)$. They present the lowest values of optical bandgap and are electrically conductive. Positive charges associated to oxygen vacancies are progressively created in these films when oxygen flow rate is increased. The film deposited with $Q(O_2) = 1.2$ sccm, close to stoichiometric WO_2, presented the lowest interface trap distributions reflecting a good quality of the WO_2/Si interface.

In zones 2 to 4, the deposition rate and target voltage decrease when $Q(O_2)$ increases from 1.95 sccm to 14 sccm. These films are all transparent with an average optical transmittance close to 80% and their optical bandgap increases with $Q(O_2)$. As a consequence, these films are electrically resistive and their electrical properties cannot be measured with the 4 probes method. The number of positive charges associated to oxygen vacancies is maximum in the film deposited with $Q(O_2) = 1.95$ sccm. Above $Q(O_2) = 1.95$ sccm, the introduced oxygen flow rate serves to fulfil oxygen vacancies so that a decrease of positive charges created in these films is observed from $Q(O_2) = 1.95$ sccm to $Q(O_2) = 8$ sccm corresponding to Zones 2 and 3. When all oxygen vacancies are fulfilled, further increase of oxygen flow rate introduced in the deposition chamber, favours the creation of negative charges in the films, as we can observe in Zone 4. According to the results of chemical composition, we can conclude that films with negative N_{ss} are stoichiometric or over stoichiometric.

Furthermore, films deposited in Zone 2, with $Q(O_2) = 1.95$ sccm, 3 sccm and 4.5 sccm, presented an important degradation of the WO_x/Si interface quality with high D_{it} values. Nevertheless, WO_x/Si interface quality is improved for films close to stoichiometric WO_3 deposited in Zones 3 and 4 with $Q(O_2) = 8$ sccm, 11 sccm and 14 sccm, for which the values of D_{it} are the lowest. As a consequence, we can say that stoichiometric films, WO_2 and WO_3, have better WO_x/Si interface quality and lowest interface trap density distribution in Hg/WO_x/Si structures.

Author Contributions: For research articles with several authors, a short paragraph specifying their individual contributions must be provided. The following statements should be used "Conceptualization, C.R. and M.G.; methodology, C.R. and J.-I.N.; formal analysis, C.R. and J.-I.N.; investigation,

J.-I.N. and C.R.; resources, C.R., W.H. and Y.M.; writing—review and editing, C.R. and J.-I.N.; visualization, J.-I.N. and C.R.; supervision, C.R.; project administration, C.R.; funding acquisition, C.R. and M.G. All authors have read and agreed to the published version of the manuscript.

Funding: This work has been supported by the PMA (Pays Montbéliard Agglomération) and the state of Côte d'Ivoire.

Institutional Review Board Statement: Not applicable.

Informed Consent Statement: Not applicable.

Data Availability Statement: All data were presented in this manuscript.

Conflicts of Interest: The authors declare no conflict of interest.

References

[1] H. Kaneko, F. Nagao, K. Miyake, Preparation and properties of the dc reactively sputtered tungsten oxide films, Journal of Applied Physics. 63 (1988) 510–517. https://doi.org/10.1063/1.340272.

[2] C.G. Granqvist, Oxide electrochromics: Why, how, and whither, Solar Energy Materials and Solar Cells. 92 (2008) 203–208. https://doi.org/10.1016/j.solmat.2006.10.027.

[3] M. Torabi Goodarzi, M. Ranjbar, Atmospheric flame vapor deposition of WO3 thin films for hydrogen detection with enhanced sensing characteristics, Ceramics International. 46 (2020) 21248–21255. https://doi.org/10.1016/j.ceramint.2020.05.215.

[4] F.G.K. Baucke, Electrochromic mirrors with variable reflectance, Solar Energy Materials. 16 (1987) 67–77. https://doi.org/10.1016/0165-1633(87)90009-8.

[5] C.G. Granqvist, A. Azens, P. Heszler, L.B. Kish, L. Österlund, Nanomaterials for benign indoor environments: Electrochromics for "smart windows", sensors for air quality, and photo-catalysts for air cleaning, Solar Energy Materials and Solar Cells. 91 (2007) 355–365. https://doi.org/10.1016/j.solmat.2006.10.011.

[6] E. Tutov, MOS structures with amorphous tungsten trioxide for capacitive humidity sensors, Semiconductors. 42 (2008) 1561–1563. https://doi.org/10.1134/S106378260813023X.

[7] K. Khojier, S. Zolghadr, F. Teimoori, S. Goudarzi, Fabrication and characterization of porous WO3 thin film as a high accuracy cyclohexene sensor, Materials Science in Semiconductor Processing. 118 (2020) 105220. https://doi.org/10.1016/j.mssp.2020.105220.

[8] D.W. Leitzke, C.M. Cholant, D.M. Landarin, C.S. Lucio, L.U. Krüger, A. Gündel, W.H. Flores, M.P. Rodrigues, R.D.C. Balboni, A. Pawlicka, C.O. Avellaneda, Electrochemical properties of WO3 sol-gel thin films on indium tin oxide/poly(ethylene terephthalate) substrate, Thin Solid Films. 683 (2019) 8–15. https://doi.org/10.1016/j.tsf.2019.05.018.

[9] V.H.V. Quy, I.-R. Jo, S.-H. Kang, K.-S. Ahn, Amorphous-crystalline dual phase WO3 synthesized by pulsed-voltage electrodeposition and its application to electrochromic devices, Journal of Industrial and Engineering Chemistry. 94 (2021) 264–271. https://doi.org/10.1016/j.jiec.2020.10.047.

[10] A. Yamamoto, Y. Abe, M. Kawamura, K. Sasaki, Effects of oxygen gettering and target mode change in the formation process of reactively RF sputtered WO x thin films, Vacuum. 66 (2002) 269–273. https://doi.org/10.1016/S0042-207X(02)00153-7.

[11] A. Monteiro, M.F. Costa, B. Almeida, V. Teixeira, J. Gago, E. Roman, Structural and optical characterization of WO3 deposited on glass and ITO, Vacuum. 64 (2002) 287–291. https://doi.org/10.1016/S0042-207X(01)00300-1.

[12] S.H. Mohamed, H.A. Mohamed, H.A. Abd El Ghani, Development of structural and optical properties of WOx films upon increasing oxygen partial pressure during reactive sputtering, Physica B: Condensed Matter. 406 (2011) 831–835. https://doi.org/10.1016/j.physb.2010.12.005.

[13] X. Xu, M.A.P. Yazdi, R. Salut, J.-M. Cote, A. Billard, N. Martin, Structure, composition and electronic transport properties of tungsten oxide thin film sputter-deposited by the reactive gas pulsing process, Materials Chemistry and Physics. 205 (2018) 391–400. https://doi.org/10.1016/j.matchemphys.2017.11.048.

[14] M. Regragui, V. Jousseaume, M. Addou, A. Outzourhit, J.C. Bernéde, B. El Idrissi, Electrical and optical properties of WO3 thin films, Thin Solid Films. 397 (2001) 238–243. https://doi.org/10.1016/S0040-6090(01)01405-5. 808 809
[15] W. Li, A. Sasaki, H. Oozu, K. Aoki, K. Kakushima, Y. Kataoka, A. Nishiyama, N. Sugii, H. Wakabayashi, K. Tsutsui, K. Natori, H. Iwai, Electron transport mechanism of tungsten trioxide powder thin film studied by investigating effect of annealing on resistivity, Microelectronics Reliability. 55 (2015) 407–410. https://doi.org/10.1016/j.microrel.2014.10.012. 810 811 812
[16] M. Raja, J. Chandrasekaran, M. Balaji, P. Kathirvel, Investigation of microstructural, optical and dc electrical properties of spin coated Al:WO3 thin films for n-Al:WO3/p-Si heterojunction diodes, Optik. 145 (2017) 169–180. https://doi.org/10.1016/j.ijleo.2017.07.049. 813 814 815
[17] Y. Xin, H. Zhou, X. Ni, Y. Pan, X. Zhang, J. Zheng, S. Bao, P. Jin, The optical properties of low infrared transmittance WO3−x nanocrystal thin films prepared by DC magnetron sputtering under different oxygen ratios, RSC Adv. 5 (2015) 57757–57763. https://doi.org/10.1039/C5RA09518B. 816 817 818
[18] A. Baltakesmez, S. Tekmen, B. Güzeldir, Temperature dependent current- and capacitance-voltage characteristics of W/n-Si structures with two-dimensional WS2 and three-dimensional WO3 interfaces deposited by RF sputtering technique, Materials Science in Semiconductor Processing. 118 (2020) 105204. https://doi.org/10.1016/j.mssp.2020.105204. 819 820 821
[19] C. Liu, Y.-M. Zhang, Y.-M. Zhang, H.-L. Lü, Interfacial characteristics of Al/Al2O3/ZnO/n-GaAs MOS capacitor, Chinese Phys. B. 22 (2013) 076701. https://doi.org/10.1088/1674-1056/22/7/076701. 822 823
[20] L.M. Terman, An investigation of surface states at a silicon/silicon oxide interface employing metal-oxide-silicon diodes, Solid-State Electronics. 5 (1962) 285–299. https://doi.org/10.1016/0038-1101(62)90111-9. 824 825
[21] C-V Characterization of MOS Capacitors Using the Model 4200-SCS Semiconductor Characterization System, Keithley Application Note, 2896, (2007). 826 827
[22] DK. Schroder, Semiconductor Material and Device Characterization, 3 rd edition, (2006). 828
[23] M. Ridaoui, Fabrication et caractérisation de MOSFET III-V à faible bande interdite et canal ultra mince, thèse N° 42401, Université des sciences et technologies de Lille, Université de Sherbrooke, Lille, (2017). 829 830
[24] F. Gao, G. Li, Y. Xia, Influence of hysteresis effect on properties of reactively sputtered TiAlSiN films, Applied Surface Science. 431 (2018) 160–164. https://doi.org/10.1016/j.apsusc.2017.07.283. 831 832
[25] A. Meeuwissen, G.B.F. Bosco, E. van der Kolk, Optical and structural characterization of Tm2O3, TmN, and TmOxNy thin films grown by direct-current reactive magnetron sputtering, Thin Solid Films. 717 (2021) 138450. https://doi.org/10.1016/j.tsf.2020.138450. 833 834 835
[26] Rossnagel S.M, Cuomo J.J., Westwood W.D, Handbook of Plasma Processing Technology, Park Ridge, New Jersey,USA, (1990). 836 837
[27] S. Habib, A. Rizk, I. Mousa, Physical parameters affecting deposition rates of binary alloys in a magnetron sputtering system, Vacuum. 49 (1998) 153–160. https://doi.org/10.1016/S0042-207X(97)00158-9. 838 839
[28] C.G. Granqvist, Handbook of Inorganic Electrochromic Materials, Elsevier, 1995. 840
[29] N.M.G. Parreira, T. Polcar, A. Cavaleiro, Characterization of W–O coatings deposited by magnetron sputtering with reactive gas pulsing, Surface and Coatings Technology. 201 (2007) 5481–5486. https://doi.org/10.1016/j.surfcoat.2006.07.017. 841 842
[30] S. Deb, Opportunities and challenges in science and technology of WO 3 for electrochromic and related applications, Solar Energy Materials and Solar Cells. 92 (2008) 245–258. https://doi.org/10.1016/j.solmat.2007.01.026. 843 844
[31] J. Tauc, R. Grigorovici, A. Vancu, Optical Properties and Electronic Structure of Amorphous Germanium, Physica Status Solidi (b). 15 (1966) 627–637. https://doi.org/10.1002/pssb.19660150224. 845 846
[32] F.P. Koffyberg, K. Dwight, A. Wold, Interband transitions of semiconducting oxides determined from photoelectrolysis spectra, Solid State Communications. 30 (1979) 433–437. https://doi.org/10.1016/0038-1098(79)91182-7. 847 848
[33] A. Hjelm, C.G. Granqvist, J.M. Wills, Electronic structure and optical properties of WO3, LiWO3, NaWO3 and HWO3, Phys. 849

Rev. B. 54 (1996) 2436–2445. https://doi.org/10.1103/PhysRevB.54.2436.

[34] J. Sánchez-González, A. Díaz-Parralejo, A.L. Ortiz, F. Guiberteau, Determination of optical properties in nanostructured thin films using the Swanepoel method, Applied Surface Science. 252 (2006) 6013–6017. https://doi.org/10.1016/j.apsusc.2005.11.009.

[35] G.A. de Wijs, R.A. de Groot, Structure and electronic properties of amorphous WO3, Phys. Rev. B. 60 (1999) 16463–16474. https://doi.org/10.1103/PhysRevB.60.16463.

[36] A. Nakamura, S. Yamada, Fundamental absorption edge of evaporated amorphous WO3 films, Appl. Phys. 24 (1981) 55–59. https://doi.org/10.1007/BF00900398.

[37] P.P. González-Borrero, F. Sato, A.N. Medina, M.L. Baesso, A.C. Bento, G. Baldissera, C. Persson, G.A. Niklasson, C.G. Granqvist, A. Ferreira da Silva, Optical band-gap determination of nanostructured WO3 film, Appl. Phys. Lett. 96 (2010) 061909. https://doi.org/10.1063/1.3313945.

[38] K. Srinivasa Rao, B. Rajini Kanth, G. Srujana Devi, P.K. Mukhopadhyay, Structural and optical properties of nanocrystalline WO3 thin films, J Mater Sci: Mater Electron. 22 (2011) 1466. https://doi.org/10.1007/s10854-011-0331-z.

[39] D.B. Migas, V.L. Shaposhnikov, V.N. Rodin, V.E. Borisenko, Tungsten oxides. I. Effects of oxygen vacancies and doping on electronic and optical properties of different phases of WO3, Journal of Applied Physics. 108 (2010) 093713. https://doi.org/10.1063/1.3505688.

[40] R. El Beainou, A. Chargui, P. Pedrosa, A. Mosset, S. Euphrasie, P. Vairac, N. Martin, Electrical resistivity and elastic wave propagation anisotropy in glancing angle deposited tungsten and gold thin films, Applied Surface Science. 475 (2019) 606–614. https://doi.org/10.1016/j.apsusc.2019.01.041.

[41] David R. Lide, CRC Handbook of Chemistry and Physics, Internet Version 2005, <http://www.hbcpnetbase.com>, CRC Press, Boca Raton, FL, 2005.

[42] I. Goldfarb, F. Miao, J.J. Yang, W. Yi, J.P. Strachan, M.-X. Zhang, M.D. Pickett, G. Medeiros-Ribeiro, R.S. Williams, Electronic structure and transport measurements of amorphous transition-metal oxides: observation of Fermi glass behavior, Appl. Phys. A. 107 (2012) 1–11. https://doi.org/10.1007/s00339-012-6856-z.

[43] R. Chatten, A.V. Chadwick, A. Rougier, P.J.D. Lindan, The Oxygen Vacancy in Crystal Phases of WO3, J. Phys. Chem. B. 109 (2005) 3146–3156. https://doi.org/10.1021/jp045655r.

[44] D. Wei, T. Hossain, N. Garces, N. Nepal, H. Meyer III, M. Kirkham, C. Eddy, J.H. Edgar, Influence of Atomic Layer Deposition Temperatures on TiO2/n-Si MOS Capacitor, Journal of Solid State Science and Technology. 2 (2013) N110–N114. https://doi.org/10.1149/2.010305jss.

[45] M. Knoll, D. Braunig, W.R. Fahrner, Generation of Oxide Charge and Interface States by Ionizing Radiation and by Tunnel Injection Experiments, IEEE Transactions on Nuclear Science. 29 (1982) 1471–1478. https://doi.org/10.1109/TNS.1982.4336389.

[46] B.J. Gordon, C-V plotting: myths and methods, Solid State Technology. 36 (1993) 57–62.

[47] C. Li, J.H. Hsieh, M.-T. Hung, B.Q. Huang, Electrochromic study on amorphous tungsten oxide films by sputtering, Thin Solid Films. 587 (2015) 75–82. https://doi.org/10.1016/j.tsf.2014.12.022.

[48] S.-H. Lee, H.M. Cheong, C.E. Tracy, A. Mascarenhas, A.W. Czanderna, S.K. Deb, Electrochromic coloration efficiency of a-WO3−y thin films as a function of oxygen deficiency, Appl. Phys. Lett. 75 (1999) 1541–1543. https://doi.org/10.1063/1.124782.

[49] J.-G. Zhang, D.K. Benson, C.E. Tracy, S.K. Deb, A.W. Czanderna, C. Bechinger, Chromic Mechanism in Amorphous WO 3 Films, J. Electrochem. Soc. 144 (1997) 2022. https://doi.org/10.1149/1.1837737.

[50] L. Boyer, O. Fruchier, P. Notingher, S. Agnel, A. Toureille, B. Rousset, Analysis of Data Obtained Using the Thermal-Step Method on a MOS Structure—An Electrostatic Approach, Industry Applications, IEEE Transactions On. 46 (2010) 1144–1150. https://doi.org/10.1109/TIA.2010.2045211.

[51] H. Sadiki, J.F. Pierson, C. Rousselot, N. Martin, G. Terwagne, Properties and electrochromic performances of reactively sputtered tungsten oxide films with water as reactive gas, Surface and Coatings Technology. 200 (2005) 232–235.

https://doi.org/10.1016/j.surfcoat.2005.02.195.